Can. J. Remote Sensing, Vol. 37, No. 1, pp. 103–111, 2011

Identifying paddy fields with dual-polarization ALOS/PALSAR data

Yuan Zhang, Cuizhen Wang, and Qi Zhang

Abstract. Accurate documentation of paddy-rice cultivation areas is valuable in estimating rice production for food security and in assessing the environmental impacts of rice ecosystems such as water consumption, soil degradation, and river eutrophication. This study explores the feasibility of dual-polarization L-band advanced land observing satellite/phased array-type L-band synthetic aperture radar (ALOS/PALSAR) imagery acquired during three growing stages in delineating paddy fields from other agricultural land uses. The study area was in the Yangtze River Delta of east China, a rapidly developing region where land has been intensively used. Among a set of arithmetic outputs of PALSAR backscatter, the amplitude ratio (HH/HV) and product (HH $\times$ HV) in the rice-transplanting and -heading stages significantly enhanced the backscatter difference between rice and nonrice fields. With these outputs, a segmentation-based decision-tree classifier successfully extracted paddy-rice fields from other land uses in the study area. Both random-point accuracy assessment and area comparison with a high-resolution Quickbird image showed that the paddy-rice map reached accuracies higher than 90%. The simplicity and generality of the approach in this study indicated that it may serve as an efficient tool for rice mapping in the highly fragmented agricultural region in southeast China.

Résumé. Il est essentiel de disposer d'une information précise sur les superficies des riziéres pour pouvoir estimer la production de riz dans le contexte de la sécurité alimentaire et pour évaluer les impacts environnementaux des écosystémes du riz comme la consommation d'eau, la dégradation du sol et l'eutrophisation des cours d'eau. Dans cette étude, on explore le potentiel des images en polarisation double du capteur PALSAR d'ALOS en bande L acquises durant trois stades de croissance du riz pour délimiter les riziéres par rapport aux autres utilisations agricoles du sol. La zone d'étude est située dans le delta du fleuve Yangtzé, dans l'est de la Chine, une région soumise á une croissance rapide oú les terres sont utilisées de façon intensive. Parmi les différents produits de rétrodiffusion PALSAR étudiés, le rapport d'amplitude (HH/HV) et le produit (HH $\times$ HV) durant les stades de la transplantation et de l'épiaison du riz ont amélioré significativement la différence dans la rétrodiffusion entre les riziéres et les autres parcelles en culture. Á l'aide de ces produits, un classifieur basé sur un arbre de décision utilisé pour fins de segmentation a permis d'extraire avec succés les riziéres des autres utilisations du sol dans la zone d'étude. Une évaluation de la précision basée sur des points aléatoires ainsi qu'une comparaison des surfaces réalisées á l'aide d'une image haute résolution de Quickbird ont montré que la carte des riziéres pouvait atteindre des niveaux de précision supérieurs á 90 %. La simplicité et l'universalité de l'approche dans cette étude démontrent que l'approche peut constituer un outil utile pour la cartographie du riz dans une région agricole hautement fragmentée dans le sud de la Chine.
[Traduit par la Rédaction]

Introduction

Paddy rice is widely planted in southeast China and accounts for more than 40% of the national crop yield (Shao et al., 2002). Rapid population growth in China demands higher rice production, while agricultural land is gradually occupied by urban development. Since the late 1970s, China's economic reform has led to intensive land-use practices in the Yangtze River Delta (Lin and Ho, 2003). Reliable rice monitoring and area estimation are therefore a critical issue for stable food production and sustainable development in this region (Pampolino et al., 2007).

Remote sensing has been applied in cropland mapping for many years. With capabilities for large-area coverage and frequent observations, optical systems such as Thematic Mapper (TM), Advanced Very High Resolution Radiometer (AVHRR), and Moderate Resolution Imaging Spectroradiometer (MODIS) acquire data at multiple spatial/spectral/

Received 16 March 2010. Accepted 18 October 2010. Published on the Web at http://pubs.casi.ca/journal/cjrs on 16 September 2011.

Y. Zhang.[1,2] Research Center of Remote Sensing and Geoscience, Northeast Institute of Geography and Agroecology, Chinese Academy of Science, Changchun 130012, Peoples' Republic of China.

C. Wang. Department of Geography, University of Missouri, Columbia, MO 65211, USA.

Q. Zhang. College of Environmental and Resources Sciences, Zhejiang University, Hangzhou 310029, Peoples' Republic of China.

[1]Corresponding author (e-mail: yuan.zhang75@gmail.com).

[2]Present address. School of Resources and Environmental Science, East China Normal University, Shanghai 200062, Peoples' Republic of China.

temporal resolutions that have been used practically in estimating crop cultivation areas at local or regional levels (Fang, 1998; Okamoto and Fukuhara, 1999; Xiao et al., 2005). However, rice mapping with optical imagery is challenging in southeast China, where paddy rice grows during a warm, humid season with frequent cloud cover and heavy rainfall. It is often difficult and sometimes impossible to acquire cloud-free optical images during critical rice-growing seasons (Wang and Huang, 2002).

Synthetic aperture radar (SAR) has become an important alternative in rice-cropping regions because of its all-weather, cloud-free observation capabilities. Most of the current satellite SAR systems, such as those on board the European Remote Sensing Satellite (ERS-1/2), Environment Satellite (Envisat), and Canadian Radar Satellite (RADARSAT 1/2), acquire C-band SAR images in single or dual polarizations. These images have been used extensively for rice monitoring in many countries (Le Toan et al., 1997; Ribbes and Le Toan, 1999; Shao et al., 2001; Park and Chi 2008). For example, ERS-1 data have been operationally applied in India for annual mapping of rice-crop acreage and production at a national scale for the past 11 years (Patel et al., 1995; Panigrahy et al., 1997; Ranganath et al., 2007). Studies in southern China also showed that Envisat ASAR data could serve as a primary data source in rice mapping and reach comparative accuracies with optical imagery (Bouvet et al., 2005; Dong et al., 2006; Chen et al., 2007). In these studies, the unique phenology and seasonality of paddy rice play a vital role in delineating it from other crops and nonvegetation land covers.

Arithmetic calculation of SAR images at horizontal (H) and vertical (V) polarizations and different frequencies (e.g., C, L, and P bands) may provide additional information in regular land-use/land-cover mapping (Bouvet et al., 2009; Wang et al., 2009). Park and Chi (2008) found that the VH/VV ratio of Envisat ASAR data was able to provide complementary information for discriminating agricultural fields from forest lands. Simard et al. (2002) added the amplitude ratio of the L-band HH JERS-1 data and C-band VV ERS-1 data as one of the image inputs in large-area mapping of tropical coastal vegetation. The overall classification accuracies in these studies were significantly higher than regular classification with raw images. Wang et al. (2009) simulated temporal variation of rice backscatter and found that L-band HH backscatter was more sensitive to rice structures than VV and therefore may be more useful in rice mapping.

More opportunities were brought into agricultural monitoring applications with the launch of the Advanced Land Observing Satellite (ALOS) by the Japan Aerospace Exploration Agency (JAXA) in 2006. The phased-array-type L-band SAR (PALSAR) on board the satellite acquires SAR imagery at 1.27 GHz frequency (L-band) at multiple polarizations (Rosenqvist et al., 2007). The PALSAR can operate in several modes: the fine-beam single (FBS) polarization (HH or VV), fine-beam dual (FBD) polarization (HH + HV or VV + VH), polarimetric (PLR) (HH + HV + VH + VV), and ScanSAR (WB) (HH or VV). In rice studies, PALSAR images reveal rich information about rice growth based on multipolarization characteristics and deeper penetration into the rice canopies of the L-band signals (Inoue et al., 2002; Wang et al., 2009). Systematic PALSAR imagery records temporal variation of rice backscatter at different rice-growth stages, which makes it promising in regional rice mapping.

The objective of this study was to test the feasibility of the L-band dual-polarization multitemporal ALOS/PALSAR imagery in identifying highly fragmented paddy fields in the Yangtze River Delta agricultural region in southeast China. A set of arithmetic calculations of the PALSAR amplitude images were processed. These arithmetic outputs at different growth stages were composed and a segmentation-based decision tree was developed to delineate paddy rice from other land covers. The rice map was validated with a fine-resolution Quickbird image and field-survey data in the study area. The approach introduced in this study was expected to provide an efficient tool for agricultural monitoring in rice-cultivation regions.

Study area and data sets

Study area

The study area was centered at 30°36′24″N, 120°44′36″E on the Hang-Jia-Hu Plain of the Yangtze River Delta, a major paddy rice cultivation region in southeast China. The Plain covers a total area of 1.2×10^4 ha in Zhejiang Province and has a typical subtropical climate with frequent rain and cloud cover during the rice-growing season. Single-season paddy rice (late June to late October) was the dominant crop in the study area. Paddy fields were typically small and highly fragmented because of intensive land-use practices such as nursery gardens, vegetable gardens, dryland crops, and rural residential settlements (**Figure 1**). The fragmented land-use/land-cover patterns made it challenging to map the rice-cultivation area and estimate rice production in this region (Skinner et al., 2001).

In one rice-growth cycle, five major development stages could be observed in the study area (Wang and Huang 2002): (1) transplanting (late June): seedlings are transplanted into fields from seedbeds; (2) tillering (early July – early August): seedlings split up but leaves are still short and sparse atop a flat water surface; (3) shooting (mid- to late August): ears start to reproduce and leaves are long and dense, so that rice canopies almost close up, with the stems clustered at the bottom; (4) heading (late September – mid-October): ears emerge on top; (5) maturing (late October): ears ripen, while leaves and stems become senescent; and (6) harvesting (mid-November): rice plants are reaped and stacked in the fields for the grain to dry.

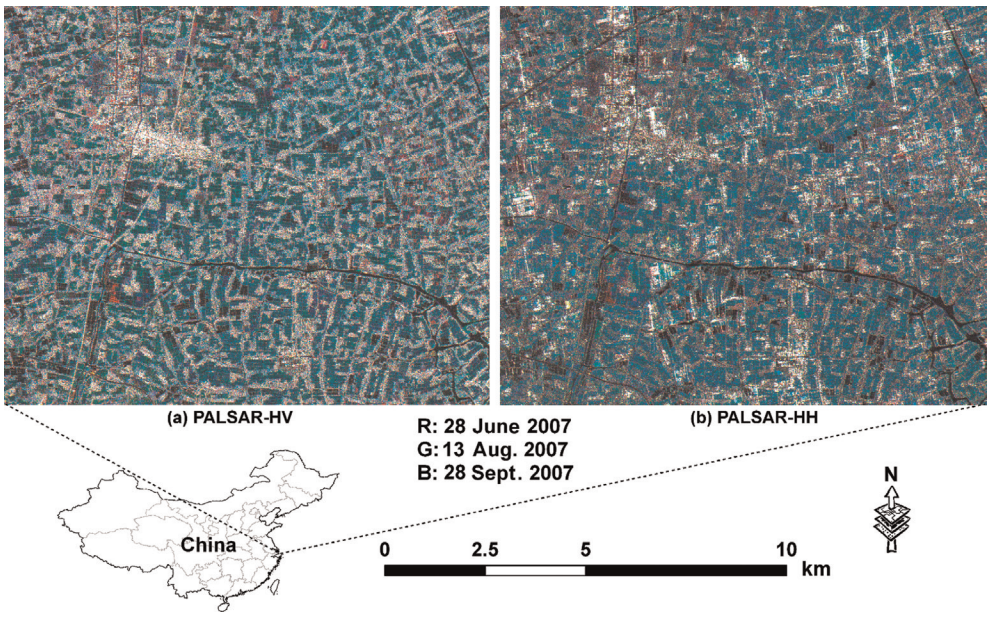

Figure 1. Three-date colour compositions of the HH and HV PALSAR images in the study area on the Hang-Jia-Hu Plain in Zhejiang Province, southeast China. The green and blue areas in the two images represent paddy-rice fields.

Data sets

Supported by the ALOS Kyoto and Carbon Initiative of JAXA, three PALSAR images in FBD mode (HH and HV) with a product version of level 1.5 were acquired in the study area on 28 June, 13 August, and 28 September 2007, i.e., during the rice transplanting, shooting, and heading stages, respectively. The images had a pixel spacing of 12.5 m, and the incident angles of the PALSAR sensor ranged from 36.7° to 38.5°.

A high-resolution (0.61 m) Quickbird image acquired on 4 November 2006 was downloaded from Google Earth. Rice fields in the image were ready for harvesting and could be easily identified at such a high resolution. Land-use change during the period of Quickbird and PALSAR image acquisition (less than 1 year) was assumed to be limited. Via image visualization and interpretation, it served as a reference to test the accuracy of the paddy-rice map derived from the PALSAR images. Additionally, a total of 82 sample sites (rice fields) were observed during three field surveys carried out on 29 June, 15 August, and 30 September 2007. These ground-truth data were effective complementary data for the purpose of validation.

Methods

PALSAR image processing: arithmetic outputs

In accordance with PALSAR image acquisitions, paddy-rice fields at three stages were shown in the photographs taken during the field survey (**Figure 2**). At the transplanting stage (late June), paddy fields were flooded with open water and therefore rice backscatter was as low as that of water bodies, while other vegetative lands such as garden vegetation and dryland crops had higher backscatter. During the shooting (mid-August) and heading (late September) stages, rice grew tall, with a closed canopy, and therefore rice backscatter increased rapidly and reached similar amplitudes to other vegetative lands. The apparent phenological variation of paddy rice resulted in a dramatic scattering difference in the three PALSAR images.

A previous study (Zhang et al., 2011) showed that the HH and HV product ($HH \times HV$) effectively increased backscatter differences among buildings, water surfaces, and vegetated fields. In this study the $HH \times HV$ product was calculated from PALSAR amplitude data in each stage. The product images at the three stages were composited and filtered with the Local Sigma Filter (Eliason and McEwen, 1990) to reduce speckle noises. **Figure 2** also shows that the apparent backscatter difference between rice and nonrice crops was observed at the transplanting and heading stages. Therefore, $HH1 \times HV1$ and $HH3 \times HV3$ were selected for rice mapping in this study. Rice canopies at each of these two stages were relatively homogeneous. $HH2 \times HV2$ was not used because rice canopies at the shooting stage varied with plant height and density because of differences in species and cultivation activities, which introduced ambiguities between rice and other vegetated covers. The PALSAR HH and HV amplitude images had a 16-bit unsigned integer format and therefore the $HH \times HV$ products could exceed the range of $[0, 2^{16}–1]$. Here we divided

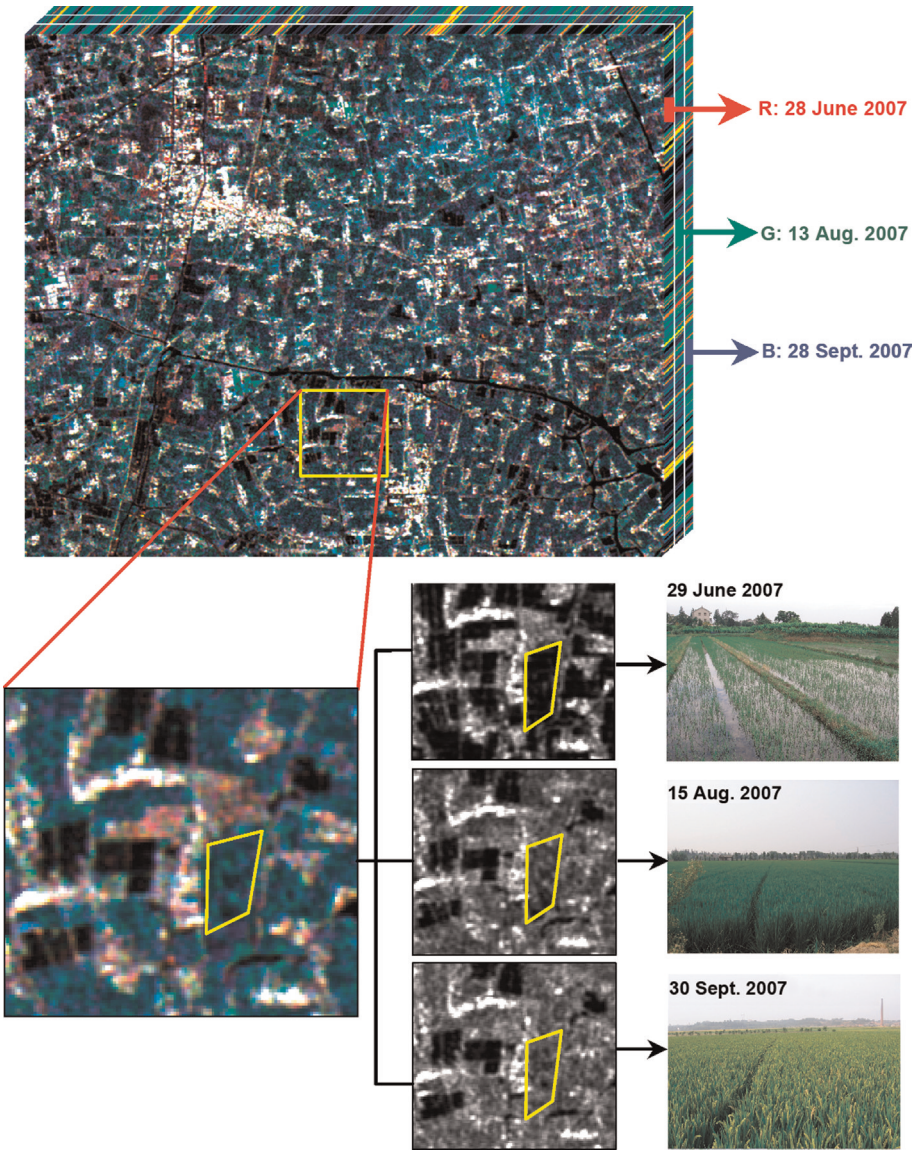

Figure 2. Three-date HH × HV composition image and an example of a rice field at three rice-growing stages (transplanting, shooting, and heading). The photographs were taken in 1–2 days before or after the ALOS/PALSAR image was acquired.

the pixel values by an adjusting factor, K ($K = 1000$ for this study) to obtain the scaled product images in 16-bit integer.

Attempts were also made in this study to examine the amplitude ratios of the HH and HV images at the three stages. We found that the amplitude ratio of the HH data on 28 September to the HV data on 28 June (HH3/HV1) significantly enhanced the separability of paddy rice from other land covers (**Figure 3**).The high HH3/HV1 values of rice backscatter came from electromagnetic interaction mechanisms between radar signals and rice fields at different stages. A the transplanting stage, rice fields were mostly flooded with open water. Scattering at this stage was dominated by specular reflection, so that the returned HH signals were limited. The HV amplitude at this stage (HV1) was extremely low. With closed rice canopies at the heading stage, rice backscatter was primarily composed of volume scattering from leaves and stems, and double-bounce scattering between rice canopies and ground surfaces (Le Toan et al., 1997; Wang et al., 2009). Rice backscatter at this stage was much higher than that at the transplanting stage, whereas that of other land covers varied less dramatically between the two stages. Consequently, HH3/HV1 of paddy fields was much higher than for other land covers. We also compared different ratios in other polarizations (HH3, HV3, HH1, and HV1) and found that the HH3/HV1 values for rice and other land covers reached a maximal difference, indicating that it was an optimal measure for enhancing the separation of rice and nonrice land covers. It was selected as

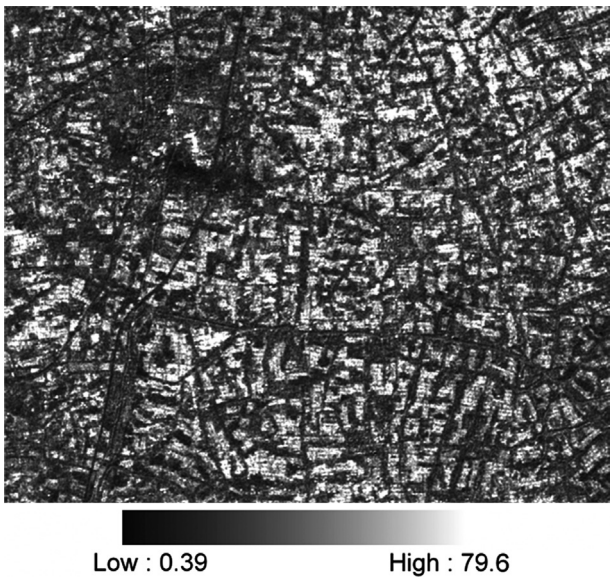

Figure 3. Amplitude ratio (HH3/HV1) of the HH image acquired on 28 September and the HV image acquired on 28 June 2007. Paddy fields are highlighted dramatically in the ratio image.

the third input layer (aside from HH1 × HV1 and HH3 × HV3) for rice mapping in the decision tree in the next section.

Rice-field identification: a segmentation-based decision tree

By visually comparing the Quickbird image and the PALSAR composite image of the three arithmetic outputs, a total of 70 sample polygons (8112 points) of five primary land-cover types in the study area were randomly selected: paddy rice (3967 points in 25 polygons), built-up areas (641 points in 10 polygons), dryland crop (274 points in 10 polygons), garden vegetation (2410 points in 13 polygons), and water surface (820 points in 12 polygons). To reduce the effects of mixed pixels, points close to field edges were not used.

These training data revealed the different backscatter features of the five land covers (**Figure 4**). Built-up areas always had the strongest backscatter amplitude, far beyond that of the vegetated and flooded land covers **(Figures 4a, 4b)**. For HH1 × HV1, flooded paddy fields at the transplanting stage had a similarly low backscatter amplitude to

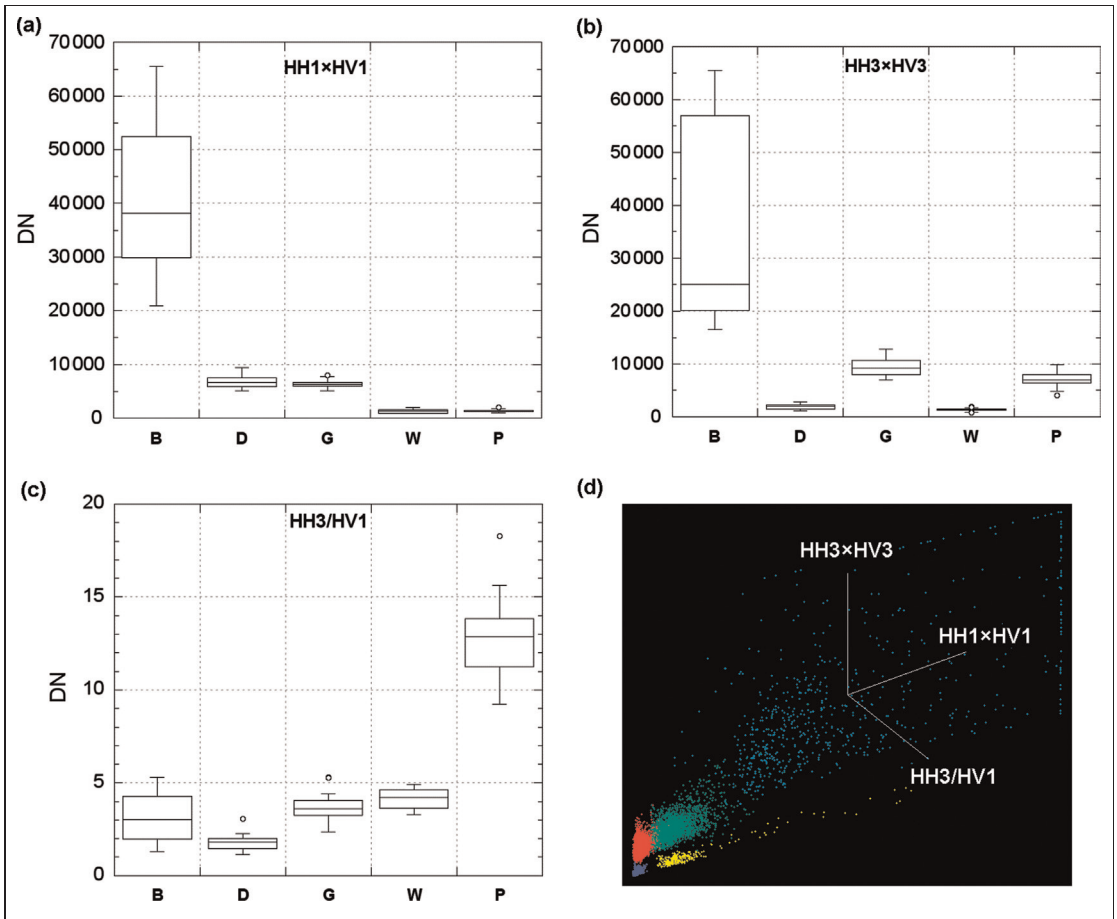

Figure 4. Features in the HH1 × HV1 (a), HH3 × HV3 (b), and HH3/HV1 (c) data, and the three-dimensional feature space (d) of sampling points of five land cover types (garden vegetation (green); paddy rice (red); dryland crop (yellow); water (blue); and built-up area (cyan)). (DN, the digital numbers in these derived images.)

water surfaces (<4000) (**Figure 4a**). For HH3 × HV3, rice scattering significantly increased with biomass in closed canopies. In this data set, rice can easily be separated from water surfaces with pixel values higher than 4500, although it mixed with garden vegetation (**Figure 4b**). For HH3/HV1, rice had remarkably higher values (>5.5) than any other land objects, which was mainly attributed to its large phenological variation (**Figure 4c**). In the three-dimensional feature space (**Figure 4d**), rice (red points) can be easily separated from built-up areas (cyan), dryland crops (yellow), and water (blue). Some rice samples were confused with garden vegetation (green). This may be due to the practice of intercropping commonly adopted in the study area, where small garden fields were often interlaced with paddy fields. The built-up areas and garden vegetation had widespread distributions in the feature space. A small number of confused points were observed between these two clusters, which may be due to mixed pixels of training data, as garden vegetation was often planted adjacent to residences. These classes were not examined further, as rice mapping was the major concern of this study.

Based on these three-dimensional feature differences among land covers, we developed a decision-tree classifier to segment image pixels into rice and nonrice using a series of customized decision rules:

$$A_{\mathrm{HH1}\times\mathrm{HV1}} < 4000, \quad \textit{and} \quad A_{\mathrm{HH3}\times\mathrm{HV3}} > 4500, \quad \textit{and} \quad AR_{\mathrm{HH3/HV1}} > 5.5 \tag{1}$$

where $A_{\mathrm{HH1}\times\mathrm{HV1}}$ and $A_{\mathrm{HH3}\times\mathrm{HV3}}$ denote the pixel values of the scaled amplitude products HH1 × HV1 and HH3 × HV3, respectively. $AR_{\mathrm{HH3/HV1}}$ denotes the pixel value of the amplitude ratio HH3/HV1.

The first criterion, $A_{\mathrm{HH1/HV1}} < 4000$, extracted flooded lands, including paddy fields and water surfaces, from the HH1 × HV1 data. The second criterion, $A_{\mathrm{HH3/HV3}} > 4500$, extracted paddy fields, other healthy vegetated fields, and urban areas that had high backscatter in the HH3 × HV3 image. The last criterion, $AR_{\mathrm{HH3/HV1}} > 5.5$, extracted paddy-rice and other vegetated fields that had a rapid backscatter increase between the two stages. When a logic "AND" operation was employed, paddy-rice fields were identified because only rice fields satisfied all three criteria. All other land covers, including dryland crops, garden vegetation, water, and built-up areas, were grouped into the nonrice class in the decision tree.

Assessment of accuracy

For comparison analysis, several subsets in the rice map were randomly selected. Reference rice maps in these subsets were manually digitized from the high-resolution Quickbird image via visual interpretation in an ArcGIS environment. These maps were assumed to be ground truth, as the Quickbird image reached a spatial resolution of 0.61 m. With acreages of the three subsets, the root mean square error (rmse) of the classified rice map was calculated:

$$\mathrm{rmse} = \sqrt{\sum_{i=1}^{n} \left(A_{\mathrm{classified}} - A_{\mathrm{reference}}\right)^2} \tag{2}$$

where $A_{\mathrm{classified}}$ and $A_{\mathrm{reference}}$ denote the rice acreage in each subset in the PALSAR-classified and Quickbird digitized rice maps, respectively; n is the number of subsets ($n = 3$ in this study).

A total of 300 validation points for each class (rice and nonrice) were also randomly collected from the PALSAR-classified rice map. Also included in the rice points were the 82 sample fields recorded during the three field surveys in 2007. Reference classes of these validation points were visually identified in the Quickbird image. A confusion matrix approach (Congalton, 1988) was then adopted to assess the accuracy of the PALSAR-classified rice map.

Results and discussion

Paddy-rice fields in the study area were classified with the decision-tree classifier developed in this study (**Figure 5**). It agreed with the field surveys that the rice fields were heavily fragmented. More built-up areas and dryland crops were observed close to the urban center in the northwest and along road infrastructures all over the study area. The rapid development of urbanization in the Yangtze River Delta in China promotes a booming infrastructure, such as highway and railway systems, which results in the reduction and fragmentation of large rice fields. Also, garden vegetation was commonly intercropped with paddy rice because of local farmers' pursuit of economic profit. These distribution features of sparse and small parcels of rice fields were recognized in the classified map. Large rice fields were observed away from urban areas. The boundaries of individual rice fields were clearly identified as shown in the three subsets randomly selected in the study area (red boxes in **Figure 5**). The a1/a2 pair represented the subset of PALSAR-classified (a1) and Quickbird-digitized (a2) rice maps in the northwest close to an urban center. Similarly, the b1/b2 pair represented the subset in the northeast, and the c1/c2 pair was in the south of the study area.

As shown in **Figure 5**, spatial distributions of paddy fields in the PALSAR-classified rice map matched well with the reference map. The acreage of paddy-rice fields in each subset was also calculated. When all three subsets were considered, the rmse of rice identification in the study area was 12.86 ha. The acreages of PALSAR-classified paddy-rice fields in the three subsets were 7.94%, 6.73%, and 7.13% lower than in the Quickbird-digitized maps, respectively (**Table 1**). The underestimation of paddy fields was primarily due to the rougher spatial resolution (12.5 m) of PALSAR compared with that of reference data Quickbird (0.61 m). Fragmented, small paddy fields

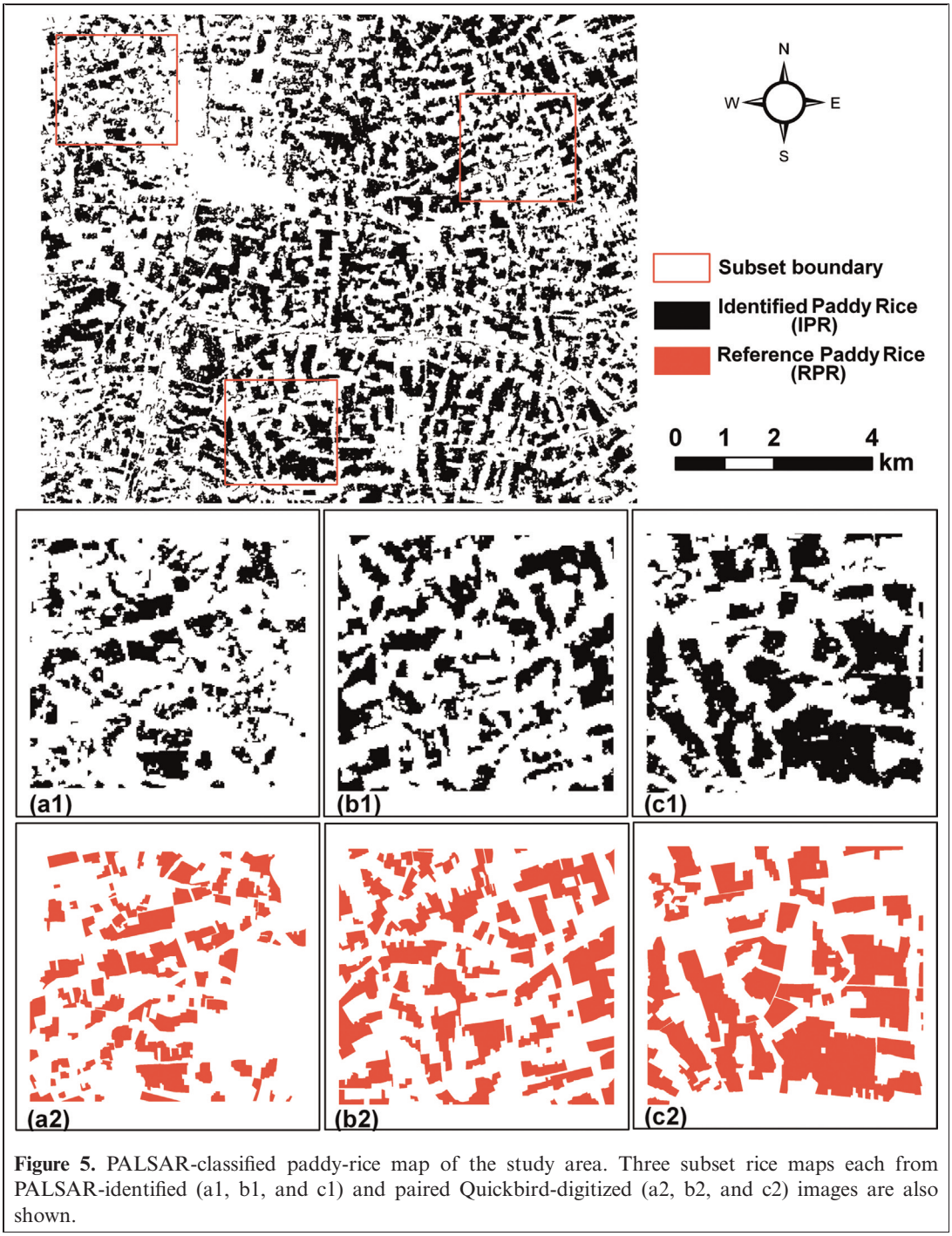

Figure 5. PALSAR-classified paddy-rice map of the study area. Three subset rice maps each from PALSAR-identified (a1, b1, and c1) and paired Quickbird-digitized (a2, b2, and c2) images are also shown.

mixed with noncrops and cannot be effectively identified in the PALSAR image. Uncertainties may also arise from a change in land use during the period when the Quickbird image was acquired in November 2006 and the PALSAR images were acquired in June–September 2007. For example, during field surveys we noticed that some paddy fields observed in 2006 were converted to aquaculture ponds in 2007. These types of land conversion, however, were limited and only involved sparse, small rice plots. As observed in our field campaign, paddy-rice planting commonly remained consistent with the previous cropping year.

Table 1. Area comparison of identified (a1, b1, and c1) with corresponding reference (a2, b2, and c2) paddy rice in three randomly selected subsets.

Subset No.	a1	a2	b1	b2	c1	c2
Area (ha)	130.03	141.24	166.52	178.53	195.64	210.67
Absolute difference (ha)	11.21		12.01		15.03	
Difference (%)	7.94		6.73		7.13	

Table 2. Error matrix of the PALSAR-identified paddy-rice map in the study area.

	Reference data				
Classified data	Nonrice	Paddy rice	Classified total	User's accuracy (%)	Conditional kappa
Nonrice	280	20	300	92.67	0.85
Paddy rice	22	278	300	93.33	0.87
Reference total	302	298	600		
Producer's accuracy (%)	93.29	92.72		Overall accuracy: 93.00%	Overall kappa: 0.86

Therefore, in the accuracy assessment of the rice map in this study, the uncertainties concerning land-use changes were assumed to be low.

With the sampling points of rice and nonrice fields randomly selected in the study area, paddy rice reached high users' and producers' accuracies of 93.33% and 92.72%, respectively. Its kppa coefficient was 0.87 (**Table 2**). Misclassified pixels were mostly found in conjoined areas between paddy fields and other land covers. Some omission pixels were located at edges of paddy fields that were shaded by nearby trees because of the slant view of the SAR systems. Commission pixels were partially attributed to the small vegetable plots between paddy fields; this intercropping is a commonly observed practice in southeast China. Furthermore, fallow or abandoned lowlands were often flooded in late June (wet season) and were covered with naturally grown grasses by late September. Temporal variation of backscatter in these areas was similar to that of paddy rice in the three-date PALSAR images, which also contributed to the commission errors of paddy rice.

This study took advantage of the unique temporal variations of rice backscatter as well as the arithmetic ratios and products of dual-polarization PALSAR images. The HH/HV and HH $\times$ HV outputs in the transplanting and heading stages of rice enhanced its backscatter difference from other land covers, which increased the feasibility of rice mapping in regions with highly fragmented rice-cropping practices. A simple segmentation-based decision-tree method used in this study reached accuracies higher than 90%. Specifically, for paddy-rice identification, the approach explored in this study is comparable to the computationally expensive classifiers used in past studies, such as the support vector machine (Zhang et al., 2009) and neural network (Shao et al., 2001).

Despite the high potential of PALSAR imagery for use in rice mapping, its widespread application is hindered by the 46-day revisit cycle of the ALOS satellite, which means that some critical cropping stages may not be monitored. This deficiency could be improved by the Advanced Land Observing Satellite-2 (ALOS-2) if it is launched successfully in the near future. The new PALSAR system on board ALOS-2 could acquire fine spatial resolution (3 m) polarimetric imagery at 14-day intervals (Kankaku et al., 2009). In the long run, the multipolarization, multimode ALOS/PALSAR data may bring great opportunities for crop mapping from an operational perspective, especially in the highly fragmented agricultural lands in the Yangtze River Delta in southeast China.

Conclusions

This study explores the feasibility of using multitemporal, dual-polarization ALOS/PALSAR images for distinguishing paddy-rice fields from other land-cover types — a simple operational method. The major scientific findings are that (*i*) the dual-polarization PALSAR images acquired during the transplanting and heading stages reveal an optimal temporal difference between the backscatter of rice and other land covers; (*ii*) the composition image of the amplitude ratio (HH/HV) and arithmetic product (HH $\times$ HV) enhances backscatter separability between paddy rice and other land covers; and (*iii*) with the two-stage dual-polarization arithmetic outputs of PALSAR images, a simple segmentation-based decision-tree classifier effectively identifies paddy-rice fields with accuracies higher than 90%. In short, this study indicates that multitemporal dual-polarization PALSAR imagery could be a promising source for paddy-rice mapping in highly fragmented agricultural lands such as the Yangtze River Delta in southeast China.

Acknowledgements

This work was supported by a research grant from the Northeast Institute of Geology and Agroecology, Chinese Academy Sciences (KZCX3-SW-NA09-05), and was funded by the National Natural Science Foundation of China (No. 41001202). The authors thank Dr. William A. Salas at Applied Geo-Solutions, LLC, U.S.A., as well as the Japan Aerospace Exploration Agency for providing the PALSAR data through the ALOS Kyoto and Carbon Initiative. Also, we thank Dr. J. Wu of Zhejiang University for providing the survey data obtained in 2007 to support the field campaign.

References

Bouvet, A., Le Toan, T., Tan, B., Li, B., He, W., and Zhang, P. 2005. Assessment of Envisat ASAR alternating polarisation data for rice mapping in Jiangsu Province, China. In *Proceedings of the 2005 Dragon Symposium: ''Mid-Term Results''*, 27 June – 1 July 2005, Sanforini, Greece. *Ed., Lacoste, H.; CD-ROM., the NASA Astrophysics Data System*, January 2006, p.36.1.

Bouvet, A., Le Toan, T., and Lam-Dao, N. 2009. Monitoring of the rice cropping system in the Mekong Delta using ENVISAT/ASAR dual polarization data. *IEEE Transactions on Geoscience and Remote Sensing*, Vol. 47, No. 2, pp. 517–526. doi: 10.1109/TGRS.2008.2007963.

Chen, J., Lin, H., and Pei, Z. 2007. Application of ENVISAT ASAR data in mapping rice crop growth in southern China. *IEEE Geoscience and Remote Sensing Letters*, Vol. 4, No. 3, pp. 431–435. doi: 10.1109/LGRS.2007.896996.

Congalton, R.G. 1988. A comparison of sampling schemes used in generating error matrices for assessing the accuracy of maps generated from remotely sensed data. *Photogrammetric Engineering and Remote Sensing*, Vol. 54, No. 5, pp. 593–600.

Dong, Y., Sun, G., and Pang, Y. 2006. Monitoring of rice crop using ENVISAT ASAR data. *Science in China Series D: Earth Sciences*, Vol. 49, No. 7, 755–763. doi: 10.1007/s11430-006-0755-0.

Eliason, E.M., and Mcewen, A.S. 1990. Adaptive box filters for removal of random noise from digital images. *Photogrammetric Engineering and Remote Sensing*, Vol. 56, No. 4, pp. 453–458.

Fang, H. 1998. Rice crop area estimation of an administrative division in China using remote sensing data. *International Journal of Remote Sensing*, Vol. 19, No. 17, pp. 3411–3419. doi: 10.1080/014311698214073.

Inoue, Y., Kurosu, T., Maeno, H., Uratsuka, S., Kozu, T., Dabrowska-Zielinska, K., and Qi, J. 2002. Season-long daily measurements of multifrequency (Ka, Ku, X, C, and L) and full-polarization backscatter signatures over paddy rice field and their relationship with biological variables. *Remote Sensing of Environment*, Vol. 81, Nos. 2–3, pp. 194–204. doi: 10.1016/S0034-4257(01)00343-1.

Kankaku, Y., Osawa, Y., Suzuki, S., and Watanabe, T. 2009. The overview of the L-band SAR onboard ALOS-2. In *Proceedings of Progress in Electromagnetics Research Symposium* (PIERS 2009), 18–21 August 2009, Moscow, Russia. Ed., J. A. Kong, The Electromagnetics Academy, Cambridge, MA,. pp. 735–738.

Le Toan, T., Ribbes, F., Wang, L.F., Nicolas, F., Ding, K.H., Kong, J.A., Fujita, M., and Kurosu, T. 1997. Rice crop mapping and monitoring using ERS-1 data based on experiment and modeling results. *IEEE Transactions on Geoscience and Remote Sensing*, Vol. 35, No. 1, pp. 41–56. doi: 10.1109/36.551933.

Lin, G.C.S., and Ho, S.P.S. 2003. China's land resources and land-use change: insights from the 1996 land survey. *Land Use Policy*, Vol. 20, No. 2, pp. 87–107. doi: 10.1016/S0264-8377(03)00007-3.

Okamoto, K., and Kawashima, H. 1999. Estimation of rice-planted area in the tropical zone using a combination of optical and microwave satellite sensor data. *International Journal of Remote Sensing*, Vol. 20, No. 5, pp. 1045–1048. doi: 10.1080/014311699213091.

Pampolino, M.F., Manguiat, I.J., Ramanathan, S., Gines, H.C., Tan, P.S., Chi, T.T.N., Rajendran, R., and Buresh, R.J. 2007. Environmental impact and economic benefits of site-specific nutrient management (SSNM) in irrigated rice systems. *Agricultural Systems*, Vol. 93, Nos. 1–3, pp. 1–24. doi: 10.1016/j.agsy.2006.04.002

Panigrahy, S., Chakraborty, M., Sharma, S.A., Kundu, N., Ghose, S.C., and Pal, M. 1997. Early estimation of rice acre using temporal ERS-1 synthetic aperture radar data — a case study for Howrah and Hooghly districts of West Bengal, India. *International Journal of Remote Sensing*, Vol. 18, No. 8, pp. 1827–1833.

Park, N.W., and Chi, K.H. 2008. Integration of multitemporal/polarization C-band SAR data sets for land-cover classification. *International Journal of Remote Sensing*, Vol. 29, No. 16, pp. 4667–4688. doi: 10.1080/01431160801947341.

Patel, N.K., Medhavy, T.T., Patnaik, C., and Hussain, A. 1995. Multi-temporal ERS-1 SAR data for identification of rice crop. *Journal of Indian Society of Remote Sensing*, Vol. 23, No. 2, pp. 33–39. doi: 10.1007/BF03007970.

Ranganath, R., Navalgund1, Jayaraman, V., and Roy, P.S. 2007. Remote sensing applications: an overview. *Current Science*, Vol. 93, No. 12, pp. 1747–1766.

Ribbes, F., and Le Toan, T. 1999. Coupling radar data and rice growth model for yield estimation. In *Proceedings of the IEEE International Geoscience and Remote Sensing Symposium (IGARSS'99)*, 28 June – 2 July 1999, Hamburg, Germany. Ed., T. I. Stein, IEEE Publications, Piscataway, NJ, pp. 2336–2338.

Rosenqvist, A., Shimada, M., Ito, N., and Watanabe, M. 2007. ALOS PALSAR: a pathfinder mission for global-scale monitoring of the environment. *IEEE Transactions on Geoscience and Remote Sensing*, Vol. 45, No. 11, pp. 3307–3316. doi: 10.1109/TGRS.2007.901027.

Shao, Y., Fan, X., Liu, H., Xiao, J., Ross, S., Brisco, B., Brown, R., and Staples, G. 2001. Rice monitoring and production estimation using multi-temporal Radarsat. *Remote Sensing of Environment*, Vol. 76, No. 3, pp. 310–325. doi:10.1016/S0034-4257(00)00212-1.

Shao, Y., Liao, J., and Wang, C. 2002. Analysis of temporal radar backscatter of rice: a comparison of SAR observations with modeling results. *Canadian Journal of Remote Sensing*, Vol. 28, No. 2, pp. 128–138.

Simard, M., De Grandi, G., Saatchi, S., and Mayaux, P. 2002. Mapping tropical coastal vegetation using JERS-1 and ERS-1 radar data with a decision tree classifier. *International Journal of Remote Sensing*, Vol. 23, No. 7, pp. 1461–1474. doi: 10.1080/01431160110092984.

Skinner, M.W., Kuhn, R.G., and Joseph, A.E. 2001. Agricultural land protection in China: a case study of local governance in Zhejiang Province. *Land Use Policy*, Vol. 18, No. 4, pp. 329–340. doi:10.1016/S0264-8377(01)00026-6.

Wang, C., Wu, J., Zhang, Y., Pan, G., Qi, J., and Salas, W.A. 2009. Characterizing L-band scattering of paddy rice in southeast China with Radiative Transfer Model and multitemporal ALOS/PALSAR imagery. *IEEE Transactions on Geoscience and Remote Sensing*, Vol. 47, No. 4, pp. 988–998. doi: 10.1109/TGRS.2008.2008309.

Wang, R.C., and Huang, J.F. 2002. *Rice Yield estimation using remote sensing data*. China Agriculture Press, Beijing, Peoples' Republic of China.

Xiao, X., Boles, S., Liu, J., Zhuang, D., Frolking, S., Li, C., Salas, W., and Moore, B. 2005. Mapping paddy rice agriculture in southern China using multi-temporal MODIS images. *Remote Sensing of Environment*, Vol. 95, No. 4, pp. 480–492.

Zhang, Y., Wang, C., Wu, J., Qi, J., and Salas, A.W. 2009. Mapping paddy rice with multi-temporal ALOS PALSAR imagery in southeast China. *International Journal of Remote Sensing*, Vol. 30, No. 23, pp. 6301–6315. doi: 10.1080/01431160902842391.

Zhang, Y., Wang, C., Chen, X., and Su, S. 2011. Support vector machine algorithm for identifying buildings using multitemporal ALOS/PALSAR data. *International Journal of Remote Sensing*. In press. doi: 10.1080/01431161.2010.519006.